# Recent advances in linear methods for sensitivity, passive control and modeling of thermo-acoustic instabilities

**By L. Magri AND M. Ihme**

## 1. Motivation and objectives

Thermo-acoustic instabilities are a challenging problem that affects aircraft gas turbines, rockets, furnaces, and other confined combustion systems (Lieuwen & Yang 2005). For these instabilities to occur, the fluctuating heat release has to be sufficiently in phase with the pressure. This leads to a thermo-acoustic oscillation, which usually displays itself as noise, vibrations, flame extinction and structural failure. It is, therefore, paramount for engineers to understand, predict and control these oscillations, and suppress them when they occur.

Many studies have demonstrated the ability of Large-Eddy Simulation (LES) to represent the flame dynamics. However, even when LES simulations confirm that a combustor is unstable, they do not provide direct information to control thermo-acoustic instabilities. Moreover, LES is computationally expensive. Low-order methods are, therefore, often developed and deployed. Network-based low-order methods model the geometry of the combustor as a network of homogeneous 1D or 2D axisymmetric acoustic elements where the acoustic problem can be solved analytically (Stow & Dowling 2001). Jump relations connect these elements, enforcing pressure continuity and mass conservation, thereby accounting for the dilatation caused by flames. The acoustic quantities in each segment are the sum of forward and backward acoustic waves, whose amplitudes and relative phases are determined such that all the jump relations and boundary conditions are satisfied. This can only be achieved for discrete values of complex eigenfrequencies.

Helmholtz models assume that the base flow, denoted by the subscript 0, is steady and solve for a Laplace-transformed wave equation for the acoustic pressure, which reads

$$\nabla \cdot \left( \frac{1}{\rho_0} \nabla \hat{p} \right) - \frac{\sigma^2}{\gamma p_0} \hat{p} = -\sigma \frac{\gamma - 1}{\gamma p_0} \hat{\mathcal{Q}}, \tag{1.1}$$

where $\hat{p}(\mathbf{x}) \exp(\sigma t)$ is the acoustic pressure, $\hat{\mathcal{Q}}(\mathbf{x}) \exp(\sigma t)$ is the heat released by the flame and $\sigma$ is the complex eigenvalue. The flame is often modeled as an acoustic element whose response is linear with respect to the acoustic field (Flame Transfer Function, FTF), i.e., $\hat{\mathcal{Q}} = \hat{\mathcal{G}} \left[ \nabla \hat{p} \right] + \hat{\mathcal{L}} \left[ \hat{p} \right]$, where $\hat{\mathcal{L}}$ and $\hat{\mathcal{G}}$ are two linear operators acting on $\hat{p}$ and its gradient, respectively.

Both network-based models and Helmholtz approaches lead, in general, to an eigenproblem that is nonlinear in the eigenvalue

$$\mathbf{N} \left\{ \sigma, \mathbf{p} \right\} \hat{\mathbf{q}} = 0, \tag{1.2}$$

where $\mathbf{N}\{\}$ is an operator acting on the eigenfunction $\hat{\mathbf{q}}$, depending nonlinearly on $\sigma$, and $\mathbf{p}$ is a vector containing the system's parameters. In this case, $\hat{\mathbf{q}} = \hat{p}$, however, $\hat{\mathbf{q}}$ can contain more variables, such as the acoustic velocity, mixture fraction, etc. The size of the

operator matrix is of the order of 10, in the case of a network-based model, or proportional to the number of nodes in the numerical mesh in the case of the Helmholtz approach, typically of the order of $10^5 - 10^6$ for industrial geometries. An important source of nonlinearity is the flame model, which introduces a characteristic time delay $\tau$ appearing as $\exp(-\sigma\tau)$ in the frequency space. Other nonlinearities in $\sigma$ may appear because of the boundary impedances (Nicoud *et al.* 2007). However, the eigenvalue problem in Eq. (1.2) is linear in the eigenfunction, $\hat{\mathbf{q}}$, as long as the nonlinear response of the flame is not accounted for.

### 1.1. *Adjoint-based sensitivity methods*

The objective is to design a combustion system that is linearly stable to thermo-acoustic oscillations over the desired operating range. The methods reviewed in this paper enable the calculation of the exact effect that a small change in the design, operating condition and introduction of a passive device have on the thermo-acoustic stability.

Thermo-acoustic systems are characterized by many parameters. In situations that are susceptible to thermo-acoustic oscillations, often only a handful of oscillation modes are unstable. Existing techniques examine how a change in one parameter affects all (calculated) oscillation modes, whether unstable or not. Adjoint techniques turn this around. In a single calculation, they examine how each oscillation mode is affected by changes in all parameters. In other words, they provide gradient information about the variation of an eigenvalue with respect to all the parameters in the model (Magri & Juniper 2013, 2014*a*; Luchini & Bottaro 2014). To study the influence of a small change in one of the many parameters of the network, the usual approach is to re-run the stability analysis for every parameter and calculate how every eigenvalue is affected. This is called the 'finite-difference' approach (Magri & Juniper 2013). On the other hand, to stabilize only the unstable eigenvalues, via adjoint methods it is possible to quantify the influence of small changes of all the network parameters only on the eigenvalues of interest. This means there is no need to re-run the stability analysis and it is possible to reduce the number of eigenproblem computations proportionally to the number of parameters of the network. In a system with a thousand parameters, therefore, adjoint methods calculate gradients about thousand times faster than finite difference methods. The same concept can be applied to the calculation of the optimal position where to place an external passive device, reducing the number of eigenproblem computations as many times as the number of grid points, which can be millions.

In this paper, we review and discuss recent developments in adjoint-based sensitivity analysis and modeling as applied to thermo-acoustics. The methods are demonstrated for combustors of increasing complexity. It is shown that adjoint methods are versatile, in that they can be used in different solvers and flame configurations, and cover diverse purposes, from sensitivity and passive control to uncertainty quantification in linear and nonlinear eigenproblems. An electrical heated Rijke tube is considered to propose a strategy for passive control of oscillations. The theoretical predictions from adjoint analysis (Magri & Juniper 2013) are validated against the experimental results of Rigas *et al.* (2016). A ducted diffusion flame is studied to show the areas of the flame that are most receptive to external species injection forcing. Control strategies by changing base-state parameters are calculated (Magri & Juniper 2014*b*). The hydrodynamic receptivity and the effect of mean-flow modifications of a turbulent bi-swirling flame combustor (Meier *et al.* 2006; Magri *et al.* 2014) is investigated. Even though this analysis does not include acoustic effects, we find that this combustor is not prone to thermo-acoustic instability because the axisymmetric longitudinal hydrodynamic mode is stable. The realistic tur-

bulent premixed swirled combustor of Palies *et al.* (2011) is then investigated to show how to apply adjoint methods to uncertainty quantification of the oscillation growth rate (Magri 2015; Magri *et al.* 2015; Silva *et al.* 2016). Via multiple scales, a thermo-acoustic stability model is developed to couple the hydrodynamic and acoustic subsystems, and the mutual influence on the stability is calculated by the intrinsic sensitivity.

Because the objective of this paper is to provide an overview of recent developments in this area of research and the capabilities of the proposed methods, the detailed numerical approaches, parameters and equations are only partially explained. Therefore, in each section, the reader is referred to relevant literature for more detailed information.

## 2. Eigenvalue sensitivity

We briefly show how to use adjoint methods to calculate the sensitivity of a nonlinear thermo-acoustic eigenvalue to all the parameters of interest. This approach is based on a Discrete Adjoint method, which is typically very accurate (see, for thermo-acoustic problems, Magri & Juniper 2013, 2014*a*,*b*). First, using matrix notation for the numerically discretized equations, we define the adjoint eigenproblem as the conjugate transpose of the direct eigenproblem in Eq. (1.2)

$$\mathbf{N}\left\{\sigma_0, \mathbf{p}_0\right\}^H \hat{\mathbf{q}}^+ = 0, \tag{2.1}$$

where $\sigma_0$ is the eigenvalue solution of Eq. (1.2). In this paper, $\hat{\phi}$ denotes the eigenfunction, or the Laplace transform, of the generic variable $\phi$. Secondly, we perturb the system's parameters as $\mathbf{p} = \mathbf{p}_0 + \delta\mathbf{p}$ and calculate numerically the perturbation operator, $\delta\mathbf{N}\{\sigma_0, \mathbf{p}\} = \mathbf{N}\{\sigma_0, \mathbf{p}\} - \mathbf{N}\{\sigma_0, \mathbf{p}_0\}$, assuming that $\sigma = \sigma_0 + \delta\sigma_1 + \delta\sigma_2$ and $\hat{\mathbf{q}} \to \hat{\mathbf{q}} + \delta\hat{\mathbf{q}}_1 + \delta\hat{\mathbf{q}}_2$, where the subscripts 1 and 2 denote the first and second order perturbations, respectively. Using Eq. (2.1), as described in Juniper *et al.* (2014); Magri (2015); Magri *et al.* (2015), yields an equation for the first-order eigenvalue drift

$$\delta\sigma_1 = -\hat{\mathbf{q}}^{+H}\delta\mathbf{N}\hat{\mathbf{q}}, \tag{2.2}$$

which is normalized by setting $\hat{\mathbf{q}}^{+H}\frac{\partial\mathbf{N}}{\partial\sigma}\Big|_{\sigma_0}\hat{\mathbf{q}} = 1$. The dependency on $\{\sigma_0, \mathbf{p}\}$ is dropped for brevity. If the eigenproblem is linear, $\mathbf{N} = \mathbf{J} - \sigma\mathbf{I}$, where $\mathbf{J}$ is the Jacobian that does not depend on $\sigma$ and $\mathbf{I}$ is the identity matrix. In this case, Eq. (2.2) simplifies to

$$\delta\sigma_1 = \hat{\mathbf{q}}^{+H}\delta\mathbf{J}\hat{\mathbf{q}}, \tag{2.3}$$

which is normalized by $\hat{\mathbf{q}}^{+H}\hat{\mathbf{q}} = 1$. If the number of components of $\mathbf{p}$ is $M$, and we are interested in the first-order sensitivity for each, Eq. (2.2) enables us to reduce the number of computations by circa $MQ$, where $Q$ is the average number of iterations needed to obtain $\delta\sigma_1$ by solving the nonlinear eigenproblem via finite difference. The second-order eigenvalue correction (Magri 2015; Juniper *et al.* 2014) reads

$$\delta\sigma_2 = -2\hat{\mathbf{q}}^{+H}\left(\frac{\partial\mathbf{N}}{\partial\sigma}\Big|_{\sigma_0}\delta\sigma_1\delta\hat{\mathbf{q}}_1 + \delta\mathbf{N}\delta\hat{\mathbf{q}}_1 + \hat{\mathbf{q}}^{+H}\frac{1}{2}\frac{\partial^2\mathbf{N}}{\partial\sigma^2}\Big|_{\sigma_0}\delta\sigma_1^2\hat{\mathbf{q}}\right). \tag{2.4}$$

The perturbed eigenfunction $\delta\hat{\mathbf{q}}_1$ is a solution of a non-homogeneous singular linear system, which can be solved, among other methods, by singular value decomposition (Magri *et al.* 2015).

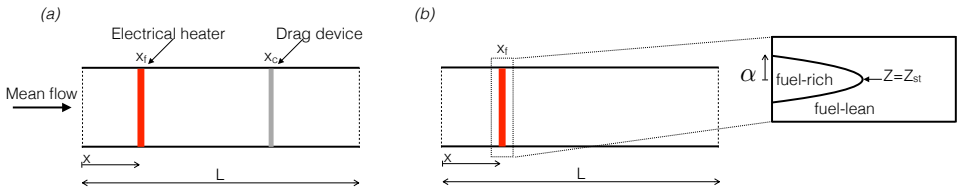


FIGURE 1. Schematic of (a) the electrical heated Rijke tube and (b) the ducted diffusion flame, in which the flame is solved in an ad-hoc domain and feeds into the acoustics through the integral of the heat release.

## 3. Passive control by an external drag device

In passive control, an object that is placed at a point in the system causes feedback at that point. Under these conditions, the sensitivities in Eqs. (2.2)-(2.3) reveal the feedback mechanism that is most effective at changing the frequency or growth rate of the system (also called structural sensitivity). In this section, we consider an electrically heated open-ended duct (Rijke tube) with fully reflective boundary conditions (Figure 1(a)). The one-dimensional thermo-acoustic problem is governed by Eq. (1.1) and the heat release is modeled by a linearized $n-\tau$ law (Magri & Juniper 2013). A Galerkin method is used to reduce the system of partial differential equations to a set of ordinary differential equations. All the numerical details can be found in Magri & Juniper (2013).

In this case, the eigenvalue, $\sigma$, is governed by a linear eigenproblem and the first-order eigenvalue drift, $\delta\sigma_1$, is given by Eq. (2.3). The state vector contains the acoustic velocity and pressure, $\hat{\mathbf{q}} = (\hat{u}, \hat{p})$, where the acoustic velocity is obtained from the momentum equation. The structural sensitivity tensor, $\mathbf{S}$, quantifies how a feedback mechanism that is proportional to the state variables affects the growth rate and frequency of the system. It is defined by setting $\delta\mathbf{J} = \mathbf{I}$ in Eq. (2.3) and, therefore, it is given by the dyadic product between the acoustic direct and adjoint eigenfunctions, $\mathbf{S} = (\hat{u}^+, \hat{p}^+)^H(\hat{u}, \hat{p})$. We consider a feedback mechanism that is proportional to the velocity and that forces the momentum equation, whose effect on the eigenvalue is given by the structural sensitivity component $S_{11}$. $\mathrm{Re}(S_{11})$ provides the sensitivity of the thermo-acoustic growth rate to a drag-exerting device placed at $x_c$. This component is positive for all values of $x$ (solid line in Figure 2), which means that, whatever value of $x$ is chosen, the growth rate will decrease if the forcing is in the opposite direction to the velocity. A damping device such as an adiabatic wire mesh would achieve this. This was tested experimentally by Rigas *et al.* (2016), who provided the first validation of the adjoint-based sensitivity predictions (circles in Figure 2).

## 4. Receptivity and base-state perturbations in diffusion flames

### 4.1. *Ducted diffusion flame*

The receptivity analysis creates a map in the flame domain of the eigenfunction's receptivity to species injection (Magri & Juniper 2014*a*). This is given by the adjoint eigenfunction. It shows the most effective regions at which to place an open-loop active device to excite the dominant thermo-acoustic mode. To illustrate this, we consider a ducted diffusion flame (Figure 1(b)), in which the combustion rate is described by equilibrium chemistry so that the chemical composition is one-to-one related to the mixture fraction, $Z$, equation. All the details can be found in Magri & Juniper (2014*b*). We per-

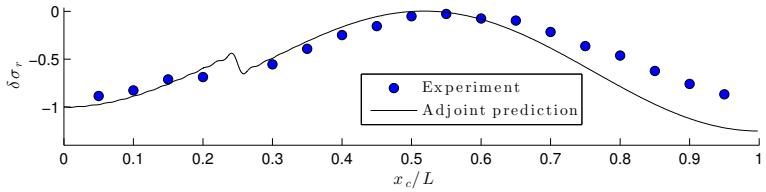


FIGURE 2. Sensitivity of the growth rate to a drag device. The heat source is located at $x_f/L = 0.25$. Adjoint theoretical predictions (solid line) against experimental results (circles, courtesy of Rigas *et al.* (2016)) normalized for comparison. The discrepancy might be due to the nonlinearity present in the experiment. More detailed explanation is reported in Magri & Juniper (2013) and Rigas *et al.* (2016).

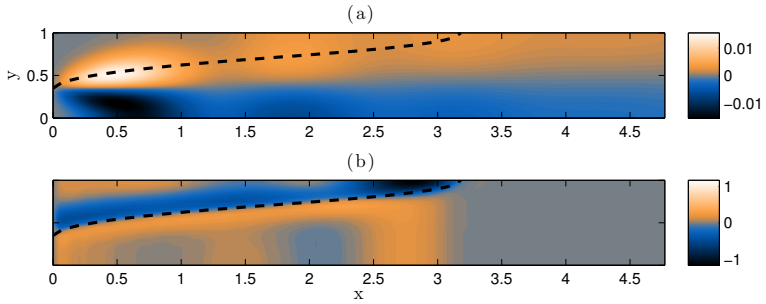


FIGURE 3. Real part of (a) the mixture-fraction eigenfunction and (b) the corresponding adjoint eigenfunction. The flame is underventilated and symmetric with respect to the centerline (Magri & Juniper 2014*b*).

turb the eigenfunction of the mixture fraction eigenfunction, $\hat{Z}$, by a forcing term that is localized in space. The direct eigenfunction represents a mixture-fraction wave traveling downstream of the duct (Figure 3(a)). The adjoint eigenfunction (Figure 3(b)) has high magnitude around the flame.

This is because species injection affects the heat release only if it changes the gradient of $\hat{Z}$ at the flame itself, which is achieved by injecting species around the flame. Its absolute value increases towards the tip of the flame, where $\nabla\hat{Z}$ is weakest. This is because mixture fraction fluctuations diffuse out as they convect down the flame, which means that open-loop forcing has a proportionately large influence on the mixture fraction towards the tip. From a practical point of view, this shows that open-loop control of the mixture fraction could be achieved by injecting species at the wall.

The change of the growth rate, $\delta\sigma_{1r}$, and the frequency, $\delta\sigma_{1i}$, due to small changes in the stoichiometric mixture fraction, $\delta Z_{st}$, and the fuel-slot geometric ratio, $\delta\alpha$, are shown in Figure 4.

$Z_{st}$ increases when the oxidizer mass fraction, $Y_o$, increases or the fuel mass fraction, $Y_F$, decreases. These results, obtained by an adjoint-based approach, have been checked against the solutions obtained via finite difference and agree to within $\sim O(10^{-9})$. Figure 4 is useful from a design point of view. For example, they reveal that at $Z_{st} = 0.12$ and $\alpha = 0.35$, changes in $Z_{st}$ strongly influence the growth rate (Figure 4(a)) but that at $Z_{st} = 0.11$ and $\alpha = 0.40$, changes in $Z_{st}$ strongly influence the frequency instead (Figure 4(b)).

Lines of constant $\delta\sigma/\delta Z_{st}$ and $\delta\sigma/\delta\alpha$ very nearly follow the grey isolines of the steady flame length shown in Figure 4. Furthermore, the sensitivities oscillate in spatial quadra-

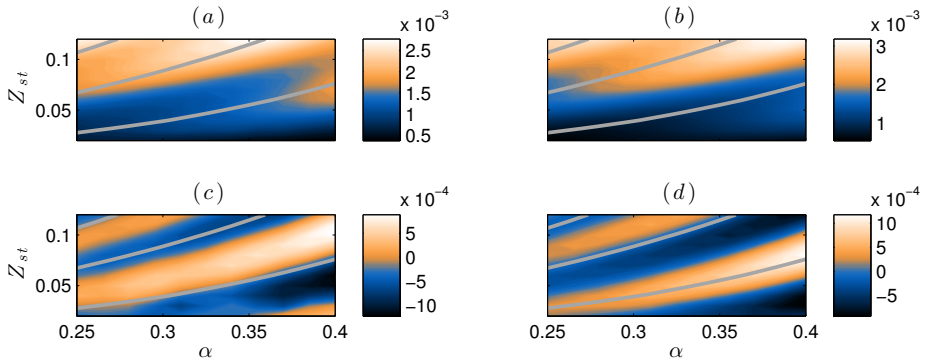


FIGURE 4. Sensitivities to base-state perturbations of $\alpha$ and $Z_{st}$: (a) $\delta\sigma_{1r}/\delta Z_{st}$, (b) $\delta\sigma_{1i}/\delta Z_{st}$, (c) $\delta\sigma_{1r}/\delta\alpha$, (d) $\delta\sigma_{1i}/\delta\alpha$ (Magri & Juniper 2014*b*). Steady-flame length contours superimposed, from bottom to top $L_f = 2, 3, 4$.

ture in parameter space (e.g. local maxima of $\delta\sigma_r/\delta Z_{st}$ lie between local maxima of $\delta\sigma_i/\delta Z_{st}$ and vice-versa). This demonstrates an inconvenient feature of thermo-acoustic instability: the influence of each parameter is exceedingly sensitive to small changes in the base state (i.e., the operating point).

### 4.2. *Hydrodynamic analysis of a dual-swirl combustor*

We study the hydrodynamic receptivity and the effect of base-state (or mean-flow) modifications of a turbulent bi-swirling $CH_4$/air flame combustor (Meier *et al.* 2006). Even though this analysis does not include acoustic effects, useful information is obtained for control of hydrodynamic instabilities, which may trigger thermo-acoustic oscillations. Details can be found in (Magri *et al.* 2014).

The mean flow is calculated by time-averaging an LES turbulent simulation (Figure 5(a,b,c)) obtained with Vida. Although the geometry is not exactly axisymmetric, by inspection of different mean-flow slices at different azimuthal locations, we notice that the flow presents axisymmetric features. Hence, we symmetrize the mean-flow data about the centerline and smooth it.

We perform a global analysis of the combusting hydrodynamic field, i.e., no acoustics is considered in this section. The axisymmetric mode $m = 0$ is convectively unstable, i.e., perturbations at the inlet are amplified and grow exponentially leaving the domain, but globally stable (Figure 5(d,e,f)). The flow is globally stable to the $m = 1$ mode, though, it is globally unstable to the $m = -1$ (Figure 5(g,h,i)) and $m = -2$ helical modes (eigenshapes of which are not shown because they resemble the $m = -1$ mode). The angular frequency of these modes are $\sigma_i = 5,002\ rad/s$ and $\sigma_i = 10,950\ rad/s$, respectively. The flow is (marginally) globally stable, but convectively unstable, to higher helical modes. The unstable $m = -1$ mode is concentrated at the reattachment point of the inner recirculation area, which is near the lateral wall far from the flame. This suggests that the active physical mechanism is mostly due to non-reacting hydrodynamic phenomena.

The adjoint eigenfunctions (Figure 5(j,k,l)) are the receptivity to open-loop external forcing. The flow is most receptive to velocity forcing, which can be caused by stochastic events/noise, but it is not as receptive to temperature forcing. The greatest receptivity straddles the inner and outer recirculation areas. The flame area is particularly receptive

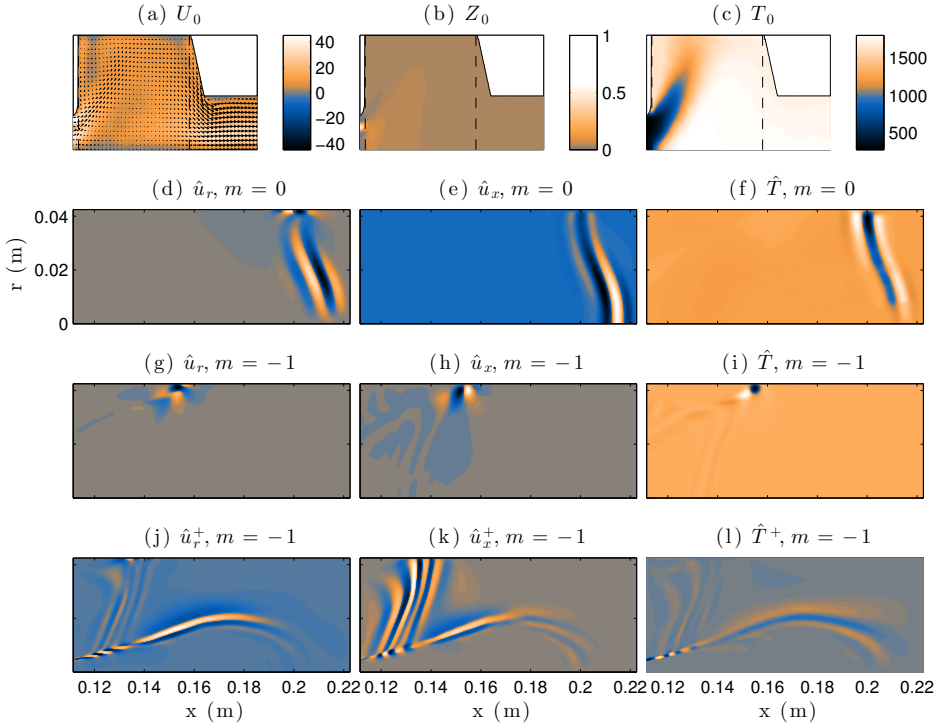


FIGURE 5. Reacting mean flow of the dual-swirl combustor. The bottom horizontal lines denote the centerline (the system is axisymmetric). (a) Velocity (m/s), the color refers to the azimuthal component; (b) mixture fraction and (c) temperature (K). The dashed box marks the border of the displayed global mode results. First row: axisymmetric $m = 0$ direct eigenfunction, which is globally stable; second row: helical $m = -1$ direct eigenfunction, which is globally unstable; third row: helical $m = -1$ adjoint eigenfunction, showing the area of highest receptivity to open loop forcing (Magri *et al.* 2014). Positive values in light color, negative values in dark. The eigenfunctions are non-dimensional and only their real part is shown.

to both temperature and velocity forcing. Open-loop forcing is most efficient there but this could be an impractical control strategy.

The highest sensitivity to feedback mechanisms acting on the mean flow, useful for practical control, is where the flow impinges on the wall and, again, along part of the recirculation area. The most efficient mechanism should react to the radial velocity and act on the radial momentum equation (Figure 6(a)). This could be achieved by modifying the wall shape with a bump. The maps in Figure 6 also suggest how and where to modify the inlet velocity profile to reduce the frequency of the coherent large-scale motion. For example, decreasing the radial component at the flame base would lower the coherent-motion frequency (Figure 6(a)).

## 5. Uncertainty quantification via an adjoint Helmholtz solver

We apply Monte Carlo simulations in order to find the Probability Density Function (PDF) of the growth rate $\sigma_r$ of the dominant thermo-acoustic mode. We study a turbulent premixed swirled combustor (Palies *et al.* 2011), shown in Figure 7(a), with plenum length

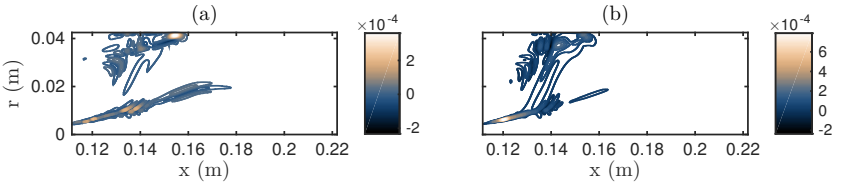


FIGURE 6. Sensitivity to mean-flow modifications to (a) radial velocity and (b) axial velocity (Magri *et al.* 2014).

$l_1 = 0.160$ m (configuration C8 in Silva *et al.* (2013)). We use a finite volume Helmholtz solver and its adjoint (Silva *et al.* 2016).

The outlet reflection coefficient (Figure 7(a)) is $R_{out} = r_0 \exp(\mathrm{i}\varphi_0)$, where $r_0 = 0.6$ and $\varphi_0 = \pi$. The flame index is $n = 1$ and the time delay is $\tau = 4.73$ ms. These uncertain design-parameters are simultaneously perturbed around their mean values assuming a uniform distribution with standard deviation of 10%. The perturbations to the eigenvalues are calculated by using the sensitivity formulae in Eqs. (2.2)-(2.4). Three methods are compared with the benchmark solution (method 0, "M0") obtained by time-consuming finite differences. In method 1, the first-order Eq. (2.3) for linear eigenproblems is utilized. In method 2, the first-order Eq. (2.2) for nonlinear eigenproblems is used. In method 3, the first-order and second-order Eqs. (2.2) and (2.4) for nonlinear eigenproblems are used. It is apparent that these methods should increasingly improve the accuracy on the uncertainty quantification.

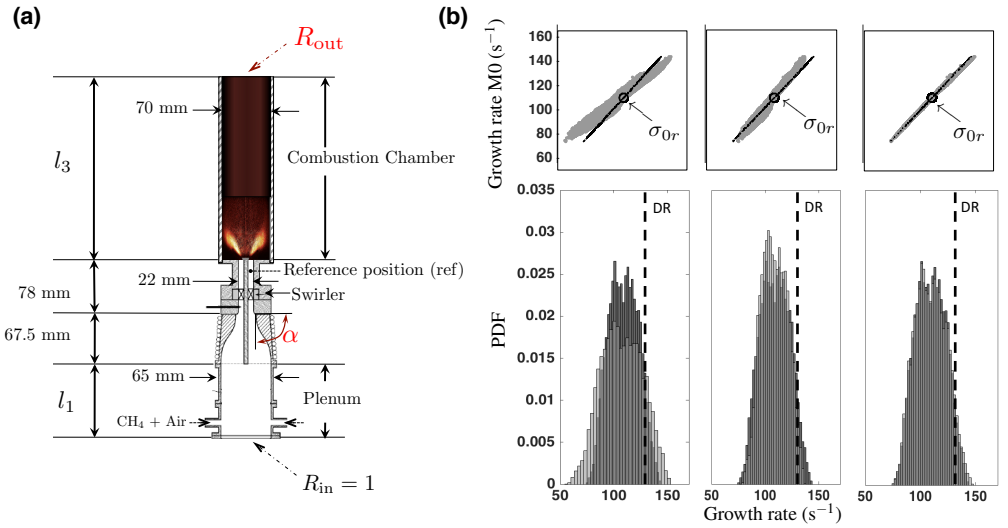


FIGURE 7. (a) Turbulent premixed swirled combustor under study for stability uncertainty quantification, adapted from Palies *et al.* (2011). (b) Distribution of the growth rates obtained with 10,000 Monte Carlo samples. Top frames: distribution of the finite-difference solution, $\tilde{\sigma}_r$ (black dots) with respect to the adjoint solution, $\sigma_r$ (grey dots). The more the scattering, the less the accuracy. Bottom frames: PDF of the perturbed growth rate. Black for Method 0 (benchmark solution by finite difference), grey for Method 1 in the left panels, Method 2 in the central panels and Method 3 in the right panels. The vertical dashed line is the combustor damping rate (DR). Adapted from Silva *et al.* (2016).

In order to compare the adjoint solutions with the finite-difference solution, the bench-

mark growth rate (vertical axis) is plotted against the growth rate $\sigma_r$ obtained from methods 1-3 (horizontal axis) in the top frames of Figure 7(b). These results confirm that the growth rate obtained from method 3 (right panels) is closest to the correct value. It means that first- and second-order terms, accounting for the nonlinearity of the eigenvalue problem, are necessary to predict the eigenvalue drift $\delta\sigma_1$ due to design-parameter uncertainties. In Silva *et al.* (2013) and Ndiaye *et al.* (2015), based on the experimental measurements of Palies *et al.* (2011), the Damping Rate (DR) of the combustor was evaluated as DR$= 125\ \mathrm{s}^{-1}$. Consequently, a combustion instability may take place if the growth rate of a given thermo-acoustic mode exceeds the damping rate ($\sigma_r >$ DR). By using an Helmholtz solver, the unperturbed eigenvalue is calculated as $\sigma_0 = 110s^{-1} + \mathrm{i}2\pi130$, i.e., the system is almost unstable. We analyze the PDF of the growth rate, which is obtained from the data generated by methods 0-3. From Figure 7(b), the PDF of the data generated by method 3 (right panels) agrees favorably with the benchmark solution (method 0 in black).

The risk factor, defined as $\int_{\mathrm{DR}}^{\infty} \mathrm{PDF}(\sigma_r)\mathrm{d}\sigma_r$, measures the probability for the system to be unstable. The risk factor obtained from method 3 (9%) is in very good agreement with the benchmark risk factor (10%) in Figure 7(b).

Growth rate uncertainty quantification is of crucial importance when studying marginally stable systems. Therefore, a single deterministic computation of $\sigma$ may not be sufficient to guarantee that the system is stable when operating. In summary, by using the first-order adjoint sensitivity for nonlinear eigenproblems (method 2, central panels in Figure 7(b)), we obtain a good estimate of the final PDF with one eigenproblem calculation versus $\sim O(10^4)$ nonlinear calculations necessary in the finite-difference method. Adding second-order corrections (method 3, right panels in Figure 7(b)), we obtain a very accurate estimate on the PDF and risk factor with one eigenproblem calculation and linear system solutions. More details can be found in Magri (2015); Juniper *et al.* (2014); Magri *et al.* (2015); Silva *et al.* (2016).

## 6. Growth rate sensitivity of the hydrodynamic and acoustic subsystems

In most thermo-acoustic models, the interaction from the acoustics to the hydrodynamics is globally simulated by a simplified convection model, such as the $n-\tau$ model, or response functions, such as the FTF, meaning that the hydrodynamic variables are not included in the state vector. The system is only one-way coupled.

To overcome this limitation, we use a low-Mach number multiple-scale method (Magri *et al.* 2014; Magri 2015; Moeck *et al.* 2009) assuming that acoustic phenomena evolve at longer spatial scales than hydrodynamic phenomena, but at the same time. Doing so, we can capture the two-way nonlinear interaction between the hydrodynamics and acoustics.

Hydrodynamic phenomena are governed by the non-dimensional continuity, momentum, energy and mixture-fraction low-Mach number equations for constant pressure flames

$$\frac{\partial \rho}{\partial t} + \nabla_x \cdot (\rho \mathbf{u}) = 0, \tag{6.1}$$

$$\frac{\partial \mathbf{u}}{\partial t} + \mathbf{u} \cdot \nabla_x \mathbf{u} + \frac{1}{\gamma\rho}\nabla_x p - \frac{1}{S_1 Re\rho}\nabla_x \cdot \bar{\boldsymbol{\tau}} = F_{ac\to hyd}, \tag{6.2}$$

$$\frac{\partial T}{\partial t} + \mathbf{u} \cdot \nabla_x T - \frac{1}{S_1 RePr\rho}\Delta_x T - DaQ_R = 0, \tag{6.3}$$

| $F_{hyd\to ac_{con}}$ | $F_{hyd\to ac_{mom}}$ | $F_{hyd\to ac_{en}}$ | $F_{ac\to hyd}$ |
|---|---|---|---|
| $-\nabla_\xi \cdot \left(\left\langle \rho^{'x}\mathbf{u}^{'x}\right\rangle_x\right)$ | $-1/\left\langle\rho\right\rangle_x \partial/\partial t \left\langle \rho^{'x}\mathbf{u}^{'x}\right\rangle_x$ | $Da\left\langle Q_{R1}\right\rangle_x$ | $-1/(\gamma\rho)\nabla_\xi p'$ |

TABLE 1. Terms coupling hydrodynamics to acoustics, $hyd \to ac$, and acoustics to hydrodynamics, $ac \to hyd$. The numeric subscripts of $Q_{R0}$ and $Q_{R1}$ refer to the orders of the heat-release asymptotic expansion.

$$\frac{\partial Z}{\partial t} + \mathbf{u}\cdot\nabla_x Z - \frac{1}{S_1 ReSc\rho}\Delta_x Z = 0, \tag{6.4}$$

where the spatial gradient $\nabla_x$ acts on the hydrodynamic spatial scale, $\mathbf{x}$, which is the shortest. The state equation is $\rho[(\,S_1-1\,)Z+1][(\,S_2-1\,)T+1]$=1, which shows that the thermodynamic pressure is constant and equal to unity when non-dimensionalized. $S_1$ is the oxidizer-to-fuel jet density ratio and $S_2$ is the adiabatic-flame-to-ambient temperature ratio. Variables and non-dimensional groups follow the common notation. This nonlinear problem can be conveniently expressed in matrix form as $\dot{\mathbf{q}}_{hyd} - \mathbf{H}(\mathbf{q}_{hyd}) = \mathbf{F}\left(\mathbf{q}\right)_{ac\to hyd}$, where $\mathbf{q}_{hyd}$=$(\rho,\mathbf{u},T,Z)^T$ is the vector of the hydrodynamic variables; $\dot{\mathbf{q}}_{hyd}$=$\partial\mathbf{q}_{hyd}/\partial t$; $\mathbf{q}$=$(\mathbf{q}_{hyd},\mathbf{q}_{ac})^T$, with $\mathbf{q}_{ac}$ being the vector of the acoustic variables; and $\mathbf{F}_{ac\to hyd}$=$(0,F_{ac\to hyd},0,0)^T$ is the forcing term (Table 1). The hydrodynamic operator, $\mathbf{H}$, is nonlinear because of the convective derivatives and reaction term.

The acoustic variables are governed by the non-dimensional continuity, momentum and energy equations

$$\frac{\partial \rho'}{\partial t} + \nabla_\xi\cdot\left(\left\langle\rho\right\rangle_x \mathbf{u}'\right) = F_{hyd\to ac_{con}}, \tag{6.5}$$

$$\frac{\partial \mathbf{u}'}{\partial t} + \frac{1}{\gamma\left\langle\rho\right\rangle_x}\nabla_\xi p' = F_{hyd\to ac_{mom}}, \tag{6.6}$$

$$\frac{\partial p'}{\partial t} + \gamma\nabla_\xi\cdot\mathbf{u}' = F_{hyd\to ac_{en}}, \tag{6.7}$$

where the spatial gradient $\nabla_\xi$ acts on the acoustic spatial scale, $\boldsymbol{\xi}$. The angle brackets $\langle\cdot\rangle_x$ denote the spatial averaging of the hydrodynamic variables over the acoustic space. This problem can be expressed as $\dot{\mathbf{q}}_{ac} - \mathbf{A}\mathbf{q}_{ac} = \mathbf{F}\left(\mathbf{q}\right)_{hyd\to ac}$, where $\mathbf{q}_{ac} = (\rho',\mathbf{u}',p')^T$ is the vector of the acoustic variables, and $\mathbf{F}_{hyd\to ac} = \left(F_{hyd\to ac_{con}},\, F_{hyd\to ac_{mom}},\, F_{hyd\to ac_{en}}\right)^T$ is the forcing term. The acoustic operator, $\mathbf{A}$, is linear. The nonlinearities are contained in the forcing term. The viscous-thermal acoustic dissipation is modeled as a sink term in the acoustic energy equation proportional to $p'$.

When linearized and Laplace-transformed, the thermo-acoustic problem can be expressed in compact form as a linear eigenproblem $\sigma\hat{\mathbf{q}} = \mathbf{J}\hat{\mathbf{q}}$, where

$$\mathbf{J} = \begin{bmatrix} \left(\frac{\delta\mathbf{H}}{\delta\mathbf{q}_{hyd}} + \frac{\delta\mathbf{F}_{ac\to hyd}}{\delta\mathbf{q}_{hyd}}\right) & \frac{\delta\mathbf{F}_{ac\to hyd}}{\delta\mathbf{q}_{ac}} \\ \frac{\delta\mathbf{F}_{hyd\to ac}}{\delta\mathbf{q}_{hyd}} & \left(\mathbf{A} + \frac{\delta\mathbf{F}_{hyd\to ac}}{\delta\mathbf{q}_{ac}}\right) \end{bmatrix}. \tag{6.8}$$

The Jacobian operator is evaluated at the base flow $\left(\mathbf{q}_{hyd,0},\mathbf{q}_{ac,0}\right)$. Even when linearized, the thermo-acoustic system is two-way linearly coupled.

The eigenfunctions and their adjoints can be combined to predict the first-order eigenvalue drift caused by a spatially localized perturbation to the system, represented by a local change $\delta\mathbf{J}$, using Eq. (2.3). We introduce the concept of intrinsic sensitivity (Magri 2015), extending the structural sensitivity used in Magri & Juniper (2013); Qadri *et al.* (2015), defined as the eigenvalue's sensitivity to intrinsic physical mechanisms, such as the interaction between subsystems. Here, the perturbation operator of the eigenvalue's

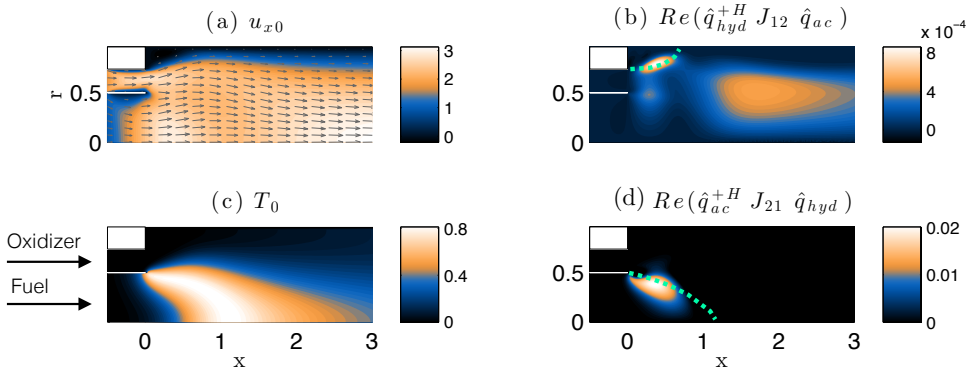


FIGURE 8. Left panels: Base-flow (a) axial velocity and (c) temperature. The velocity direction is shown with arrows in (a). Right panels: Growth-rate sensitivity (b) to intrinsic hydrodynamic feedback feeding the momentum equation, the maximum straddles the recirculation-boundary (upper dashed line) and (d) sensitivity to the hydrodynamics through acoustic mechanisms, the maximum straddles the stoichiometric line (lower dashed line). These panels depict only the most significant portion of the entire combustor and all the quantities are non-dimensional (Magri *et al.* 2014).

sensitivity Eq. (2.3) is the Jacobian itself, i.e., $\delta\mathbf{J}{=}\epsilon\mathbf{J}$, where $\epsilon \ll 1$. This enables us to identify the regions of the flow where the hydrodynamic and acoustic subsystems are active and quantify how they affect the overall thermo-acoustic stability. When the flow is laminar, the real part of Eq. (2.3) provides a map showing the regions to which the thermo-acoustic stability is sensitive to hydrodynamic and acoustic physical mechanisms.

### 6.1. *Application to a coaxial jet diffusion combustor*

Details on the numerical method and non-dimensional parameters can be found in Magri (2015); Magri *et al.* (2014). In this laminar case, the mean flow (Figure 8(a,c)) is a steady solution of the governing Eqs. (6.1)-(6.4) and it is labeled the base flow.

On the one hand, the combusting hydrodynamic flow, when the coupling forcing terms are set to zero, is globally stable. The dominant eigenvalue is $\sigma{=}{-}0.100 + \mathrm{i}1.041$. On the other hand, the acoustics, when the linearized low-Mach number flow is not coupled through forcing terms, are close to instability. The eigenvalue is $\sigma{=}{-}0.00031 + \mathrm{i}0.630$, which is close to the first organ-pipe resonance, as expected.

When two-way coupled, the low-Mach number flow and acoustics become unstable, with dominant eigenvalue $\sigma{=}0.102 + \mathrm{i}0.731$. The angular frequency is close to the acoustic frequency; the instability is driven by acoustic effects because the unstable mode is primarily acoustic (not shown). In this stability framework, the hydrodynamics is simulated and interacts with the acoustics.

We can study the effect that the acoustics has on the hydrodynamic stability, which is exactly given by the intrinsic sensitivity map $\delta\sigma_1/\epsilon = \hat{\mathbf{q}}^{+H}_{hyd}\mathbf{J}_{12}\hat{\mathbf{q}}_{ac}$. This is a spatial function and $\mathbf{J}_{12}$ is the coupling operator from the acoustics to the hydrodynamics (top-right component of the matrix in Eq. (6.8)) through the acoustic pressure gradient (fourth term in Table 1). This expression quantifies by how much a small perturbation to the acoustic field $\sim\epsilon\mathbf{J}_{12}\hat{\mathbf{q}}_{ac}$ changes the thermo-acoustic eigenvalue of the coupled system through hydrodynamic processes ($\hat{\mathbf{q}}^{+H}_{hyd}$). The real part of this quantity is shown in Fig-

ure 8(b). We note that the highest sensitivity straddles the recirculation region at the top left corner. The acoustics is acting as an extra feedback momentum source, enhancing the hydrodynamic sensitivity, which is, indeed, often close to the recirculation boundary (Luchini & Bottaro 2014). (From a hydrodynamic standpoint, this signifies that the acoustics cannot be viewed as an external forcing.) Changes in the coupling from the acoustics to the hydrodynamics here will have the most influence on this mode. However, this is only one component of the intrinsic sensitivity and the coupling from acoustics to hydrodynamics is not the dominant mechanism. The maximum growth rate drift is $\delta\sigma_{1r}\sim O(10^{-4})$.

Following the same line of reasoning, we study the effect that the hydrodynamics has on the stability through acoustic mechanisms, whose intrinsic sensitivity is $\delta\sigma_1/\epsilon = \hat{\mathbf{q}}_{ac}^{+H}\mathbf{J}_{21}\hat{\mathbf{q}}_{hyd}$, where $\mathbf{J}_{21}$ is the coupling term from the hydrodynamics to the acoustics (bottom-left component of the matrix in Eq. (6.8)). This formula quantifies by how much a small perturbation to the hydrodynamic field $\sim\epsilon\mathbf{J}_{21}\hat{\mathbf{q}}_{hyd}$ changes the thermo-acoustic eigenvalue of the coupled system through acoustic processes ($\hat{\mathbf{q}}_{ac}^{+H}$). This map is depicted in Figure 8(d). The maximum value is $\delta\sigma_{1r}\sim O(10^{-2})$. The region of high sensitivity straddles the stoichiometric line, where most of the heat is released by the flame. This shows that a small change in the coupling from hydrodynamics to acoustics causes a larger stability drift, i.e., $\delta\sigma_{1r}\sim O(10^{-2})$, than a small change in the coupling from the acoustics to the hydrodynamics, i.e., $\delta\sigma_{1r}\sim O(10^{-4})$. In other words, small changes of the hydrodynamic feedback greatly change the flame response to acoustic perturbations which, in turn, have great influence on the thermo-acoustic stability.

## 7. Conclusions

The advantage of adjoint techniques applied to thermo-acoustics is that, in few calculations, one can predict accurately how the growth rate and frequency of thermo-acoustic oscillations are affected either by all possible passive control elements in the system or by all possible changes to its base state or design-parameters.

First, adjoint sensitivity analysis is applied to an electrically heated Rijke tube for passive control of oscillations. The optimal mechanism should force the momentum equation in the opposite direction to the velocity perturbation and it should be placed at either end of the duct. An adiabatic mesh would achieve this. Each adjoint sensitivity analysis is obtained with a single adjoint calculation and is validated against experimental data, which is available in literature.

Secondly, a ducted diffusion flame is considered. The flame adjoint eigenfunction reveals that the thermo-acoustic system is most receptive to open-loop species injection towards the tip of the flame. The receptivity map is useful when designing open-loop strategies for control/excitation of thermo-acoustic oscillations. The sensitivity to base-state perturbations reveals the sensitivity to perturbations in the combustion parameters, which in this case are the stoichiometric mixture fraction, $Z_{st}$, and the fuel slot to duct width ratio, $\alpha$. Although these can be found with classical finite difference calculations, using the adjoint equations significantly reduces the number of computations without affecting the (first-order) accuracy. These are the easiest parameters to change in an experiment, although control with these would be delicate because of the sensitivity's oscillatory patterns, which make thermo-acoustic stability exceedingly sensitive to the operating condition.

Thirdly, the hydrodynamic receptivity and the effect of mean-flow modifications of

a turbulent bi-swirling flame combustor is investigated. We find that this combustor is not prone to thermo-acoustic instability because the axisymmetric longitudinal hydrodynamic mode is stable. A shape modification of the combustor's wall is proposed to stabilize the first helical mode, which is hydrodynamically unstable. This result provides gradient information that can be embedded in optimization algorithms to design an optimal controller or shape modification. Acoustic analysis and thermo-acoustic coupling is left for future work.

Fourthly, the first- and second-order eigenvalue sensitivities are applied to a turbulent premixed swirled combustor, the thermo-acoustic stability of which is modeled by a Helmholtz solver. The adjoint algorithm is applied to predict the probability for the system to be unstable (risk factor) through a Monte Carlo uncertainty quantification method. The overall risk factor and probability density function are very well predicted by the adjoint method. The number of nonlinear eigenproblems solved is reduced by a factor equal to the number of Monte Carlo samples which, in this case, is of the order of $O(10^4)$ when first-order analysis is performed.

Fifthly, using a multiple-scale asymptotic method, general equations for axisymmetric thermo-acoustic systems in low-Mach number combustors are derived. When the acoustics evolve at longer spatial scales than the hydrodynamics, but at the same time, the linearized dynamics between the hydrodynamic and acoustic subsystems is two-way coupled. The growth-rate sensitivity of a coaxial jet diffusion flame combustor is studied. Although the hydrodynamic and acoustic systems are stable, when coupled together they become unstable. By introducing the concept of intrinsic sensitivity, the exact first-order effect that the acoustics has on the hydrodynamic sensitivity is that of an extra momentum source enhancing the region of high hydrodynamic sensitivity. The hydrodynamics greatly influences the overall thermo-acoustic stability's sensitivity straddling the flame. This reveals that the active physical mechanism is thermo-acoustic.

Adjoint sensitivity methods have the potential to open up new possibilities for control, optimization and uncertainty quantification of thermo-acoustic instabilities.

## Acknowledgments

The support from NASA grant #NNM13AA11G and Ford-Stanford Alliance project #C2015-0590 are gratefully acknowledged. L.M was supported until September 2015 by the ERC grant ALORS #2590620 under the supervision of Prof. M. P. Juniper. L.M. is grateful to Prof. W. Polifke for having sponsored his visit, where some of the ideas of section 5 originated. Collaborations and interactions with Dr. C. Silva, Dr. M. Bauerheim, Dr. Y.-C. See and Prof. F. Nicoud are greatly appreciated.

## REFERENCES

Juniper, M. P., Magri, L., Bauerheim, M. & Nicoud, F. 2014 Sensitivity analysis of thermo-acoustic eigenproblems with adjoint methods. *Proceedings of the Summer Program*, Center for Turbulence Research, Stanford University, pp. 189–198.

Lieuwen, T. C. & Yang, V. 2005 *Combustion Instabilities in Gas Turbine Engines: Operational Experience, Fundamental Mechanisms, and Modeling*. American Institute of Aeronautics and Astronautics.

Luchini, P. & Bottaro, A. 2014 Adjoint equations in stability analysis. *Annu. Rev. Fluid Mech.* **46**, 1–30.

Magri, L. 2015 Adjoint methods in thermo-acoustic and combustion instability. PhD thesis, University of Cambridge.

Magri, L., Bauerheim, M., Nicoud, F. & Juniper, M. P. 2015 Sensitivity analysis and uncertainty quantification of nonlinear eigenproblems in thermo-acoustics: application to an annular combustor. Submitted to *J. Comput. Physics*.

Magri, L. & Juniper, M. P. 2013 Sensitivity analysis of a time-delayed thermo-acoustic system via an adjoint-based approach. *J. Fluid Mech.* **719**, 183–202.

Magri, L. & Juniper, M. P. 2014*a* Adjoint-based linear analysis in reduced-order thermo-acoustic models. *Int. J. Spray Combust. Dyn.* **6** (3), 225–246.

Magri, L. & Juniper, M. P. 2014*b* Global modes, receptivity, and sensitivity analysis of diffusion flames coupled with duct acoustics. *J. Fluid Mech.* **752**, 237–265.

Magri, L., See, Y. C., Ihme, M. & Juniper, M. P. 2014 Multiple-scale adjoint sensitivity analysis of hydrodynamic / thermo-acoustic instability in turbulent combustion chambers. *Proceedings of the Summer Program*, Center for Turbulence Research, Stanford University, pp. 199–208.

Meier, W., Duan, X. R. & Weigand, P. 2006 Investigations of swirl flames in a gas turbine model combustor II. Turbulence-chemistry interactions. *Combust. Flame* **144**, 225–236.

Moeck, J., Oevermann, M., Klein, R., Paschereit, C. O. & Schmidt, H. 2009 A two-way coupling for modeling thermoacoustic instabilities in a flat flame Rijke tube. *Proc. Combust. Inst.* **32** (1), 1199–1207.

Ndiaye, A., Bauerheim, M. & Nicoud, F. 2015 Uncertainty quantification of thermoacoustic instabilities in a swirled stabilized combustor. *ASME Turbo Expo, GT2015-44133*.

Nicoud, F., Benoit, L., Sensiau, C. & Poinsot, T. 2007 Acoustic Modes in Combustors with Complex Impedances and Multidimensional Active Flames. *AIAA J.* **45** (2), 426–441.

Palies, P., Durox, D., Schuller, T. & Candel, S. 2011 Nonlinear combustion instability analysis based on the flame describing function applied to turbulent premixed swirling flames. *Combust. Flame* **158** (10), 1980–1991.

Qadri, U. A., Chandler, G. J. & Juniper, M. P. 2015 Self-sustained hydrodynamic oscillations in lifted jet diffusion flames: origin and control. *J. Fluid Mech.* **775**, 201–222.

Rigas, G., Jamieson, N. P., Li, L. K. B. & Juniper, M. P. 2016 Experimental sensitivity analysis and control of thermoacoustic systems. Submitted to *J. Fluid Mech.*.

Silva, C. F., Nicoud, F., Schuller, T., Durox, D. & Candel, S. 2013 Combining a Helmholtz solver with the flame describing function to assess combustion instability in a premixed swirled combustor. *Combust. Flame* **160** (9), 1743–1754.

Silva, C. F., Runte, T., Polifke, W. & Magri, L. 2016 Uncertainty quantification of growth rates of thermoacoustic instability by an adjoint Helmholtz solver. *ASME Turbo Expo, 2016-GT-57659*.

Stow, S. R. & Dowling, A. P. 2001 Thermoacoustic oscillations in an annular combustor. *ASME Turbo Expo, 2001-GT-0037*.